Human Molecular Genetics, 2010, Vol. 19, No. 22 ***4385–4398***
doi:10.1093/hmg/ddq361
Advance Access published on August 31, 2010

A point mutation in the dynein heavy chain gene leads to striatal atrophy and compromises neurite outgrowth of striatal neurons

Kerstin E. Braunstein[1,†,‡], Judith Eschbach[2,3,‡], Krisztina Ròna-Vörös[1,‡], Rana Soylu[4], Elli Mikrouli[4], Yves Larmet[2,3], Frédérique René[2,3], Jose-Luis Gonzalez De Aguilar[2,3], Jean-Philippe Loeffler[2,3], Hans-Peter Müller[1], Selina Bucher[5], Thomas Kaulisch[5], Heiko G. Niessen[5], Julia Tillmanns[5], Kristina Fischer[6], Birgit Schwalenstöcker[1], Jan Kassubek[1], Bernd Pichler[6], Detlef Stiller[5], Åsa Petersen[4], Albert C. Ludolph[1,‡] and Luc Dupuis[2,3,*,‡]

[1]Department of Neurology, University of Ulm, Ulm, Germany, [2]INSERM, U692, Laboratoire de Signalisations Moléculaires et Neurodégénérescence, Strasbourg F-67085, France, [3]Université de Strasbourg, Faculté de Médecine, UMRS692, Strasbourg F-67085, France, [4]Translational Neuroendocrine Research Unit, Department of Experimental Medical Research, Lund University, Lund, Sweden, [5]*In-vivo* Imaging, Target Discovery Research, Boehringer Ingelheim Pharma GmbH & CO- KG, Biberach, Germany and [6]Laboratory for Preclinical Imaging and Imaging Technology of the Werner Siemens-Foundation, Department of Radiology, Eberhard Karls University of Tübingen, Röntgenweg 13, 72076 Tübingen, Germany

Received July 13, 2010; Revised and Accepted August 22, 2010

The molecular motor dynein and its associated regulatory subunit dynactin have been implicated in several neurodegenerative conditions of the basal ganglia, such as Huntington's disease (HD) and Perry syndrome, an atypical Parkinson-like disease. This pathogenic role has been largely postulated from the existence of mutations in the dynactin subunit p150^{Glued}. However, dynactin is also able to act independently of dynein, and there is currently no direct evidence linking dynein to basal ganglia degeneration. To provide such evidence, we used here a mouse strain carrying a point mutation in the dynein heavy chain gene that impairs retrograde axonal transport. These mice exhibited motor and behavioural abnormalities including hindlimb clasping, early muscle weakness, incoordination and hyperactivity. *In vivo* brain imaging using magnetic resonance imaging showed striatal atrophy and lateral ventricle enlargement. In the striatum, altered dopamine signalling, decreased dopamine D1 and D2 receptor binding in positron emission tomography SCAN and prominent astrocytosis were observed, although there was no neuronal loss either in the striatum or substantia nigra. *In vitro*, dynein mutant striatal neurons displayed strongly impaired neuritic morphology. Altogether, these findings provide a direct genetic evidence for the requirement of dynein for the morphology and function of striatal neurons. Our study supports a role for dynein dysfunction in the pathogenesis of neurodegenerative disorders of the basal ganglia, such as Perry syndrome and HD.

*To whom correspondence should be addressed at: INSERM U692, Faculté de Médecine, bat 3, 8^{e} étage, 11 rue Humann, Strasbourg F-67085, France. Tel: +33 368853091; Fax: +33 368853065; Email: ldupuis@unistra.fr
†Present address: Department of Pathology, Johns Hopkins University School of Medicine, 558 Ross Research Building, 720 Rutland Avenue, Baltimore, MD 21205, USA.
‡The authors wish it to be known that, in their opinion, the first three authors should be regarded as joint First Authors and are listed in alphabetical order and that A.C.L. and L.D. are joint Senior Authors.

INTRODUCTION

Axonal transport is a bidirectional process through which materials and signals are exchanged between the neuronal cell body and the synapse. Retrograde axonal transport is mediated by the cytoplasmic molecular motor dynein which functions in association with a multiprotein regulatory complex called dynactin (1). Loss of the dynein/dynactin function is thought to be an important factor in the pathogenesis of neurodegenerative diseases (2,3). Indeed, impairment of retrograde axonal transport appears to be one of the earliest pathogenic events during neurodegeneration (1), and transgenic inhibition of retrograde axonal transport in motor neurons is sufficient to drive the degeneration of these neurons (4,5). The involvement of dynactin in neurodegenerative diseases is supported by the discovery of mutations in the dynactin subunit p150^{Glued} in familiar forms of motor neuron disease, including amyotrophic lateral sclerosis and distal spinal and bulbar muscular atrophy (6–8), as well as in Perry syndrome, a rare atypical form of Parkinson's disease resistant to L-DOPA (9,10). *In vitro*, the G59S mutation in p150^{Glued} leads to abnormal cytoskeletal dynamics accompanied by toxic protein aggregation (11). *In vivo*, moderate neuron-specific overexpression of mutant dynactin causes motor neuron disease in mice (12–14).

The mechanisms underlying the toxicity of mutant p150^{Glued} are still elusive, because dynactin is able to regulate not only the function of dynein but also that of kinesin-2 (15). Thus, dynactin disruption disables both anterograde and retrograde trafficking (16). Furthermore, dynactin may also act, independently of its role in cellular transport, as a docking protein and has been recently suggested to affect gene transcription through direct modulation of transcription factors (17,18). Despite this emerging large array of dynactin functions, it remains postulated, although largely unproven, that dynactin mutations lead to neurodegeneration through impairment of the dynein function. Several lines of evidence suggest that dynein itself is a modifier of the degeneration of striatal neurons in Huntington's disease (HD), a neurodegenerative disorder caused by an expanded CAG repeat in the *huntingtin* gene. First, dynein, as well as p150^{Glued}, are binding partners of huntingtin and of huntingtin-associated protein 1 (HAP1) (19,20). Second, the activity of the dynein motor is positively regulated by wild-type huntingtin, and strongly decreased by the HD-associated expansion in the polyglutamine repeat domain of huntingtin (21,22). However, the effects of pathogenic huntingtin on axonal transport are widespread by affecting both anterograde and retrograde fast axonal transport (23). Thus, direct genetic evidence linking retrograde axonal transport, in particular dynein, and striatal degeneration is still lacking.

The aim of this study was to provide such evidence. For this, we took advantage of the existence of mouse strains bearing point mutations in the dynein heavy chain gene (*dync1h1*) (24). The *legs at odd angles* (*loa*) mutation represents a F580Y mutation, while the *Cramping* (*Cra*) mutation converts tyrosine 1055 to a cysteine (Y1055C). Both mutations are located in the domain involved in homodimerization of the molecular motor. Both of these mutations impair the ability of dynein motors to sustain fast retrograde transport in situations of cellular stress and lead to decreased retrograde transport in adult dynein mutant motor neurons (24,25). The phenotype of dynein mutant mice has been characterized in the peripheral nervous system, with the occurrence of a proprioceptive sensory neuropathy (26–28), but there are currently no study focusing on the central nervous system of these animals. An initial report suggested that dynein mutant mice displayed lower motor neuron degeneration, but we and others failed to reproduce these findings (26–28). In particular, we performed a longitudinal analysis of the neuromuscular phenotype of *Cra*/+ mice up to 24 months of age and found no evidence of motor neuron degeneration in these animals (27).

Here, we show that the *Cramping* dynein mutation in mice leads to distinctive signs of striatal dysfunction. Furthermore, dynein mutant striatal neurons showed profound abnormalities in neurite outgrowth *in vitro*. These findings strongly support a pathophysiological function for dynein in degenerative diseases of basal ganglia including HD and Perry syndrome.

RESULTS

The motor phenotype of *Cra*/+ mice is characterized by early muscle weakness, progressive incoordination and hyperactivity

We first performed a battery of motor and behavioural tests in mice bearing the *Cramping* mutation in the dynein heavy chain gene (*Cra*/+). In our laboratory, *Cra*/+ mice showed reduced total and forelimb muscle grip strength as early as 3 months of age (Fig. 1A), and suffered from an impairment in motor coordination that mildly increased with ageing, as observed using an accelerating rotarod test (Fig. 1B). *Cra*/+ mice displayed increased open field exploratory behaviour as revealed by increased track length and average velocity (Fig. 1C). No differences were observed in the number of rearings, indicating normal vertical behaviour (data not shown). The level of anxiety appeared similar between *Cra*/+ mice and their wild-type littermates as assessed using the elevated plus maze paradigm (Fig. 1D). In the Morris water maze test, *Cra*/+ mice tended to spend more time in reaching the platform at 12, but not 3, months of age, when compared with wild-type animals. This was likely due to impaired motor incoordination rather than to spatial memory deficits since the observed difference between genotypes was annulled when considering the distance swum by the mice (Fig. 1E). Taken together, *Cra*/+ mice display muscle weakness and incoordination with increased open field activity in the absence of obvious spatial working memory deficits.

Cra/+ mice present with striatal atrophy and lateral ventricle enlargement

Our present findings suggest that the phenotype of *Cra*/+ mice is broader than the pure proprioceptive neuropathy previously documented and could result from damage to central areas in the brain that control movement. In fact, hyperactivity and progressive motor incoordination are also distinctive features observed in mice expressing pathological forms of huntingtin or after ablation of D1 dopamine receptor expressing cells, both paradigms affecting the striatum (29–32). Forebrain, but

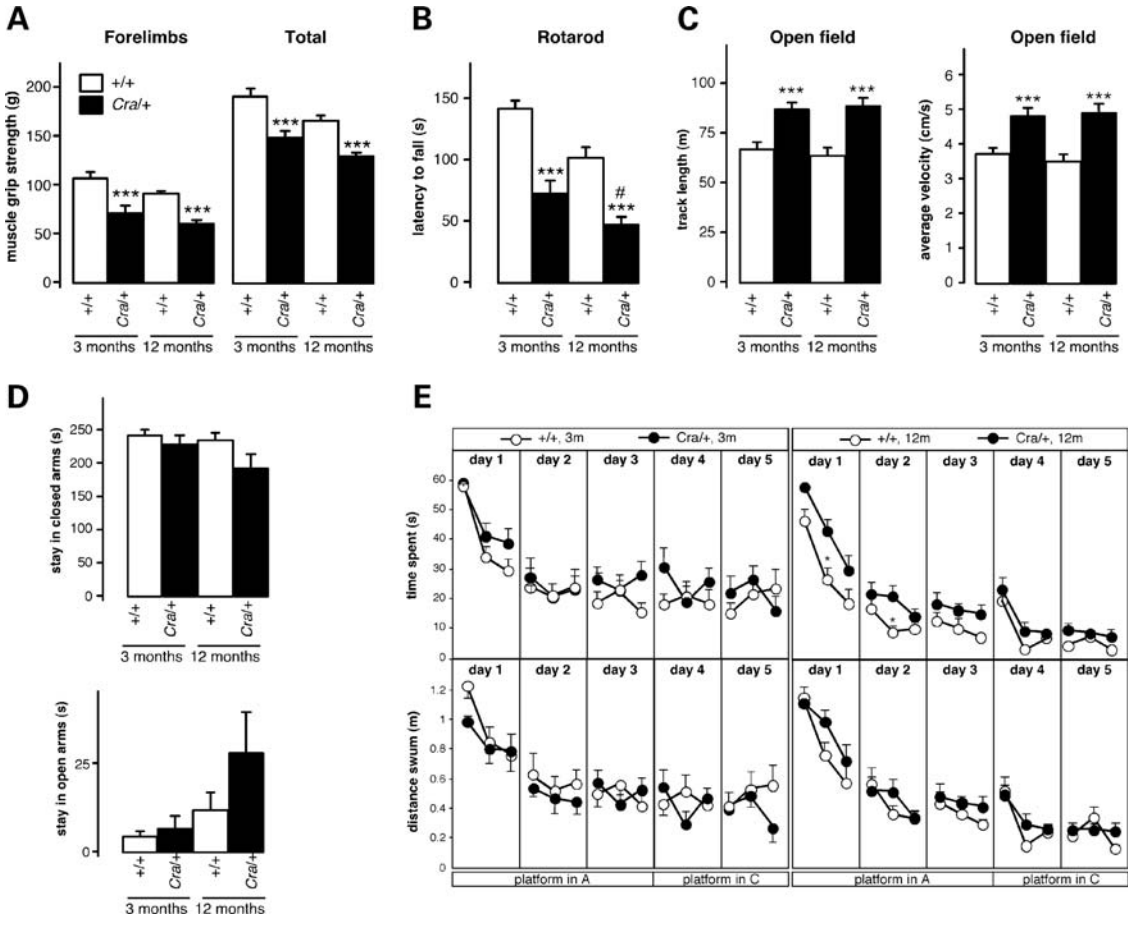

Figure 1. Locomotor and behavioural abnormalities in *Cra*/+ mice. (**A**) Grip muscle strength of forelimbs (left panel) and all limbs (right panel) in wild-type mice (+/+) and heterozygous *Cra*/+ mice at 3 and 12 months of age. $^{***}P < 0.001$ versus corresponding wild-type ($n = 12$ mice per group). (**B**) Latency to fall in an accelerating rotarod test in wild-type mice (+/+) and heterozygous *Cra*/+ mice at 3 and 12 months of age. $^{***}P < 0.001$ versus corresponding wild-type, $^{\#}P < 0.05$ versus 3-month-old *Cra*/+ mice ($n = 12$ mice per group). (**C**) Track length (left panel) and average velocity (right panel) in an open field test in wild-type mice (+/+) and heterozygous *Cra*/+ mice at 3 and 12 months of age. $^{***}P < 0.001$ versus corresponding wild-type ($n = 12$ mice per group). (**D**) Time spent in closed arms (upper panel) and open arms (lower panel) in an elevated plus maze test (during a 300 s session) by wild-type mice (+/+) and heterozygous *Cra*/+ mice at 3 and 12 months of age. Non-significant differences ($n = 12$ mice per group). (**E**) Time spent (upper panels) and distance swum (lower panel) to reach the hidden platform in a Morris water maze test by wild-type mice (+/+) and heterozygous *Cra*/+ mice at 3 (left panel) and 12 (right panel) months of age. The platform was in position A during the first 3 days of the test, and then moved to position C for the last 2 days. Six trials were performed per day, and each point is the mean of two consecutive trials. $^{*}P < 0.05$ versus corresponding wild-type in time spent and non-significant differences in distance swum ($n = 12$ mice per group).

not hindbrain, wet weight was decreased in *Cra*/+ mice (Fig. 2A), suggestive of atrophy. The striatum and cerebral cortex of *Cra*/+ mice appeared grossly normal using haematoxylin/eosin staining (Fig. 2B), and the cortical layer organization was preserved (Fig. 2C), suggesting that the defect was not due to abnormal cortical development. *In vivo* brain imaging using magnetic resonance imaging (MRI) showed a significant reduction in the volume of the *Cra*/+ mice striata at both 5 and 10 months of age (Supplementary Material, Figs S1 and S2D–E), while, concomitantly, the volumes of the lateral ventricles were significantly increased (Fig. 2D and F). Thus, the mutation in dynein leads to striatal atrophy in mice.

Progressive astrocytosis in the absence of neurodegeneration in the striatum

Reactive astrocytosis represents a typical marker of neuronal stress and is often a sign of an underlying pathology. Interestingly, reactive astrocytosis, as revealed by glial fibrillary acidic protein (GFAP) immunoreactivity (Fig. 3A), was dramatically increased in the striatum of 8-month-old *Cra*/+ mice, and this increase was even higher at 18 months of age (Fig. 3B). Consistent with this observation, striatal GFAP mRNA levels as measured using RT–qPCR were higher in *Cra*/+ mice than in wild-type littermates at 8 months, but not at 4 months of age (Fig. 3C). To determine whether astrocytosis was associated to neurodegeneration, we determined the total number of DARPP-32 (dopamine- and cAMP-regulated phosphoprotein of a molecular weight of 32 kDa) positive medium spiny neurons (MSNs), the neuronal population comprising more than 95% of striatal neurons, using stereological analysis. The analysis of DARPP-32 positive MSNs showed a non-significant trend towards decreased number at 6 months of age (Fig. 4). These data show that the phenotype of dynein mutant mice is rather due to neuronal dysfunction than due to neurodegeneration in the striatum.

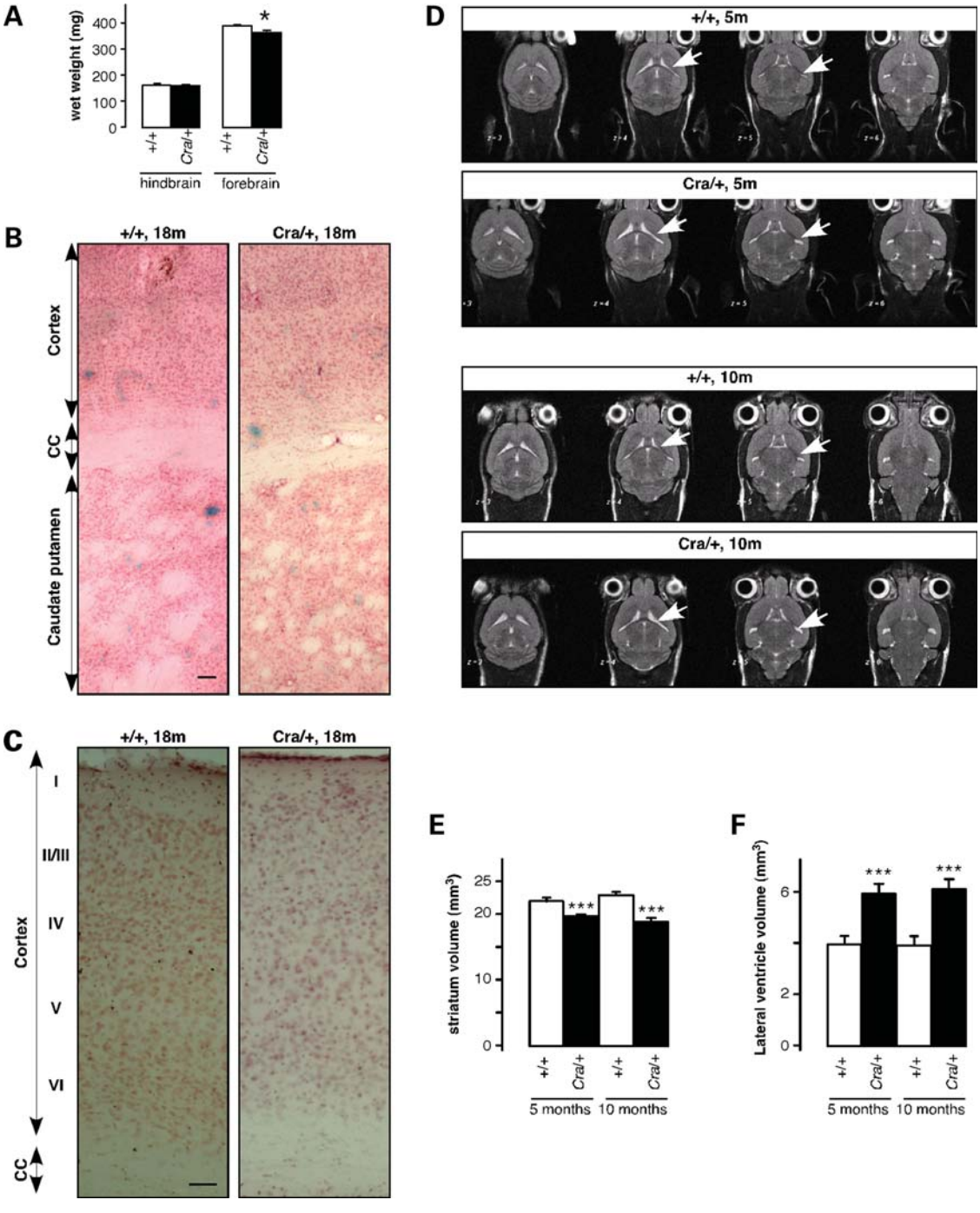

Figure 2. Striatal atrophy in *Cra*/+ mice. (**A**) Wet weight of hindbrain (left) and forebrain (right) of wild-type mice (+/+, empty columns) and heterozygous *Cra*/+ mice (black columns) at 12 months of age. $^{*}P < 0.05$ versus corresponding wild-type ($n = 4$ mice per group). (**B**) Low magnification photomicrographs of haematoxylin and eosin staining of wild-type (+/+) and heterozygous *Cra*/+ brains at 18 months of age. CC, corpus callosum. Scale bar = 100 μm. (**C**) Higher magnification of B showing the aspect of the six layers of the cortex. Scale bar = 50μm. (**D**) Representative horizontal T2-weighted MRI slices of a wild-type (+/+) and *Cra*/+ mouse at 5 and 10 months of age. Note the enlargement of the lateral ventricles (white arrows) of the *Cra*/+ mouse. (**E**) Striatal volume of wild-type (+/+, empty columns) and heterozygous *Cra*/+ mice (black columns) at 5 (left) and 10 (right) months of age. $^{***}P < 0.001$ versus corresponding wild-type ($n = 20$ mice per group). (**F**) Lateral ventricle volume of wild-type (+/+, empty columns) and heterozygous *Cra*/+ mice (black columns) at 5 (left) and 10 (right) months of age. $^{***}P < 0.001$ versus corresponding wild-type ($n = 20$ mice per group).

Altered dopamine signalling and D1 receptor binding in the striatum of *Cra*/+ mice

Our histological observations in the striatum argue in favour of neuronal dysfunction that could eventually lead to motor disturbances. To test this hypothesis, we analysed the expression of a series of genes directly involved in the striatal function. D1, but not D2, dopamine receptor mRNA levels were decreased in 8-month-old *Cra*/+ mice as shown using RT–qPCR (Fig. 5A). D1 receptor expressing cells synthesize

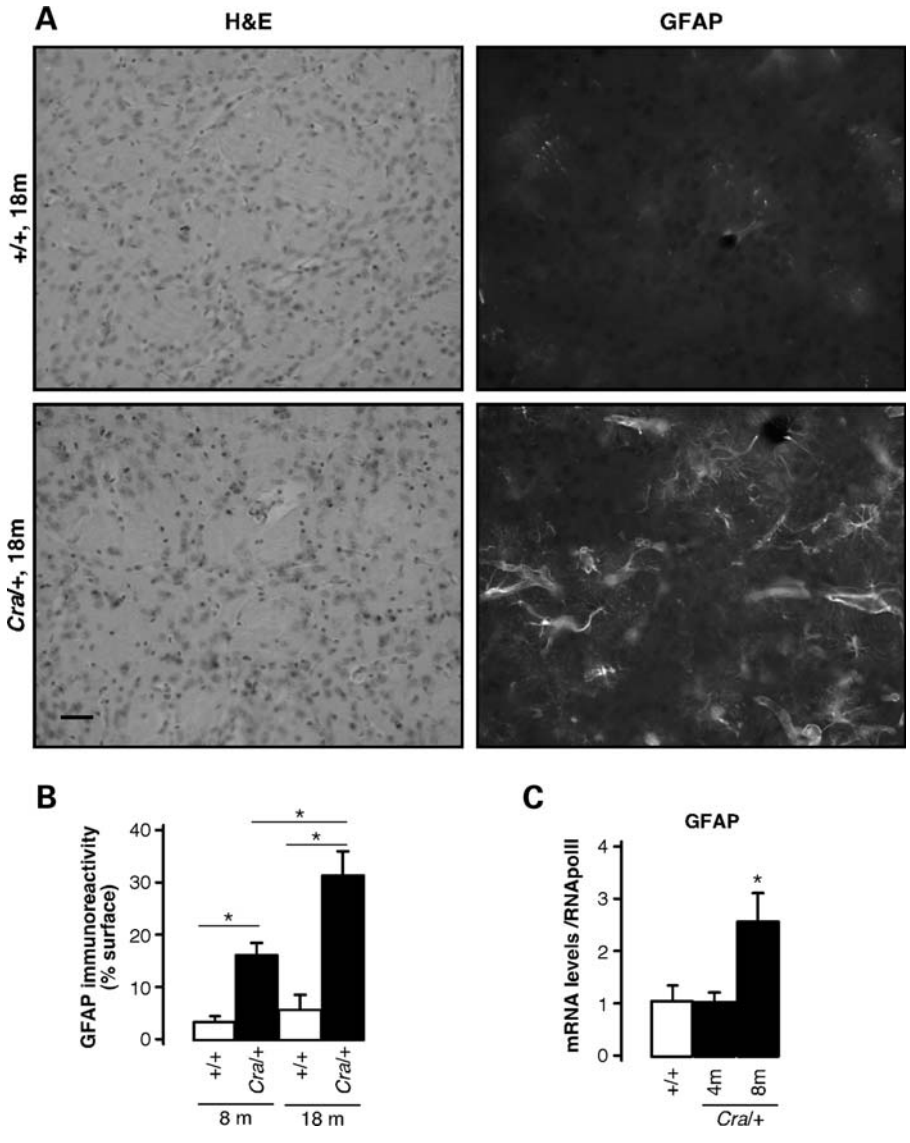

Figure 3. Progressive striatal astrocytosis in *Cra*/+ mice. (**A**) Representative microphotographs showing haematoxylin/eosin staining (left panels) and GFAP immunoreactivity (right panels) in the striatum from wild-type mice (+/+, upper panels) and heterozygous *Cra*/+ mice (lower panels) at 18 months of age. Scale bar = 25 μm. (**B**) Quantification of the surface occupied by GFAP positive cells in the striatum from wild-type mice (+/+) and heterozygous *Cra*/+ mice at 8 and 18 months of age. Data are expressed as percentage of the total surface in the picture. $^{*}P < 0.05$ versus indicated condition ($n = 5$ mice per group). (**C**) mRNA levels of GFAP in the striatum from wild-type mice (+/+) and heterozygous *Cra*/+ mice at 4 and 8 months of age. $^{*}P < 0.05$ versus wild-type ($n = 5$–7 mice per group).

substance P, whereas D2 receptor expressing cells synthesize pre-proenkephalin. Thus, substance P, but not pre-proenkephalin, mRNA levels appeared decreased in 8-month-old *Cra*/+ mice (Fig. 5A), which corroborates the selective down-regulation of the expression of D1 dopamine receptors in striatal neurons. It is therefore tempting to propose that *Cra*/+ mice suffer from D1 receptor striatal dysfunction that could underlie the motor disturbances observed in these animals. To directly determine whether this is the case, we performed positron emission tomography (PET) analysis of the binding of the D1 receptor selective ligand [^{11}C] SCH-23390 (Fig. 5B). Quantification of [^{11}C] SCH-23390 showed a decrease of the signal in the brains of *Cra*/+ mice (Fig. 5C), which further reinforces the presence of striatal dopaminergic impairment. We extended our D1-PET scans by using [^{18}F] Fallypride, a high-affinity selective dopamine D2/3 receptor ligand with the advantage of long half-life compared with [^{11}C] Raclopride (33). We observed a significant reduction of [^{18}F] Fallypride uptake in the striatum of *Cra*/+ mice compared with wild-type animals (Fig. 5D), lending further support for the involvement of the striatal dopaminergic system in the *Cra*/+ pathogenesis.

Lack of involvement of brain-derived neurotrophic factor and dopaminergic degeneration in the striatal phenotype of dynein mutant mice

The defect mediated by the dynein mutation in the striatum could be either intrinsic to the MSN or be triggered by extrinsic abnormalities in striatal afferences or efferences.

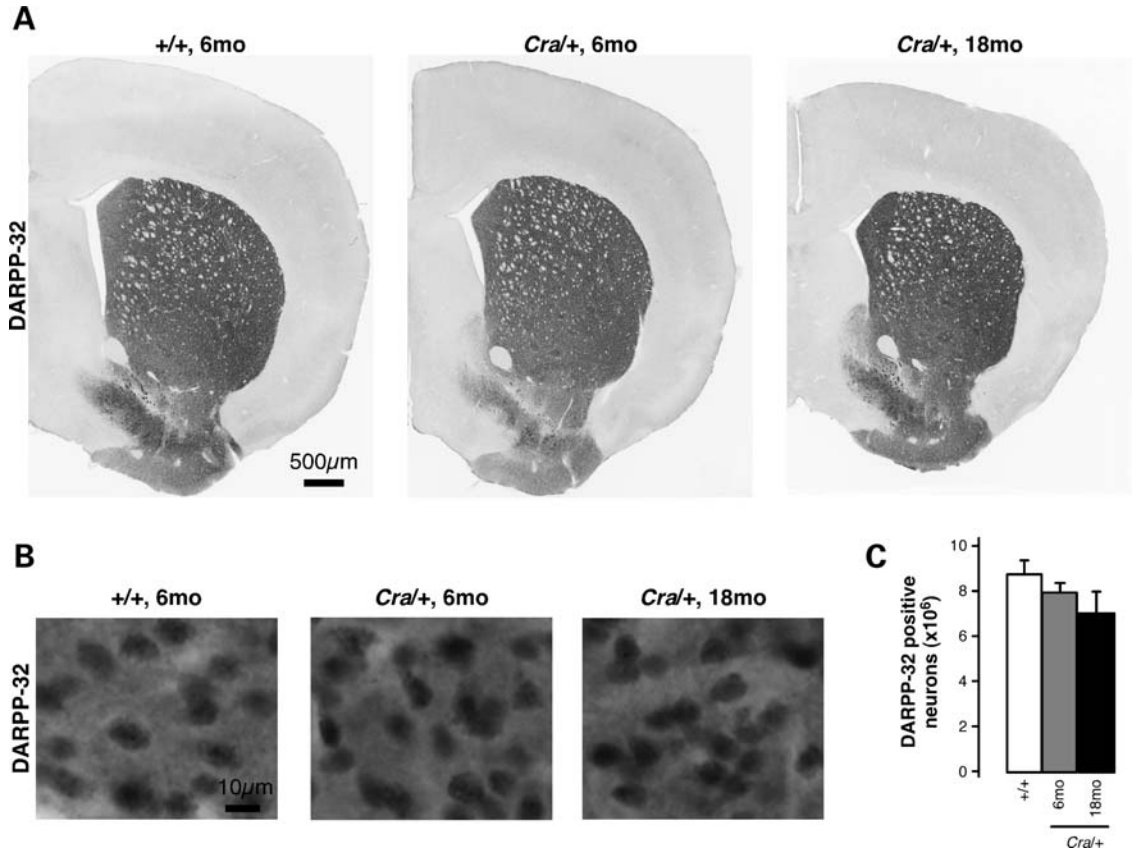

Figure 4. No significant neuronal loss in the striatum of *Cra*/+ mice. (**A** and **B**) Representative photographs of striatal sections processed for DARPP-32 immunohistochemistry from wild-type mice (+/+) at 6 months of age as well as heterozygous *Cra*/+ mice at 6 and 18 months of age. (**C**) Stereological estimations of the total number of DARPP-32 positive neurons in the unilateral striatum did not reveal any statistically significant differences between the groups ($n = 4–6$ mice per group).

Given that dynactin mutations have been associated with the Parkinson-like disease Perry syndrome (10), we hypothesized that the dynein mutation could lead to the degeneration of substantia nigra dopaminergic neurons. However, stereological assessments of tyrosine hydroxylase (TH) positive neuronal cells revealed similar numbers in the wild-type and *Cra*/+ substantia nigra pars compacta (Supplementary Material, Fig. S2) and TH staining of dynein mutant striatum appeared normal (data not shown), demonstrating that striatal atrophy is not a consequence of dopaminergic degeneration. Next we hypothesized that trophic factor deprivation of striatal neurons led to striatal atrophy. Brain-derived neurotrophic factor (BDNF), the major trophic factor for this neuronal population, is produced in the cortex and anterogradely transported to the striatum. Cortical BDNF ablation leads to a roughly similar striatal atrophy and behavioural impairment than the dynein mutation (34,35). At the mRNA level, BDNF expression was not decreased, but increased at 6 months of age in the cortex of *Cra*/+ mice (Supplementary Material, Fig. S3A). BDNF levels appeared normal in the striatum of these mice using ELISA (Supplementary Material, Fig. S3B), suggesting that BDNF was appropriately produced and targeted to the striatum. The dynein mutation could also lead to a decreased cellular response of dynein mutant neurons to BDNF exposure. Indeed, exocytosis and endocytosis, which are dynein-dependent events, appear indispensable for BDNF signal transduction (36,37). A major target of BDNF is increased DARPP-32 transcription (38) and major transcriptional responses occur 3–4 h after exposure to BDNF (39). DARPP-32 induction appeared similar between +/+, *Cra*/+ and *Cra/Cra* primary striatal neurons treated with BDNF during 4 h (Supplementary Material, Fig. S3C), suggesting that the dynein mutation did not massively impair the BDNF response of these neurons. In all, neither dopamine nor BDNF deprivation appeared to be a primary cause of dynein mutant striatal phenotype.

Cell autonomous defect in dynein mutant striatal neurons

To determine whether dynein mutant striatal neurons were intrinsically abnormal, we first studied their survival *in vitro*. Cultured embryonic striatal neurons of +/+, *Cra*/+ and *Cra/Cra* embryos showed similar survival as assessed by MTT assays (Fig. 6A), by cell counting (Fig. 6B) and by DNA (Fig. 6C) or RNA (Fig. 6D) yields of cultured neurons. Moreover, gene expression of neuronal markers such as neurofilament subunits NF-H and NF-M or DARPP-32 was identical between all three genotypes (Fig. 6E). Despite normal survival in culture, dynein mutant striatal neurons showed a profoundly abnormal dendritic

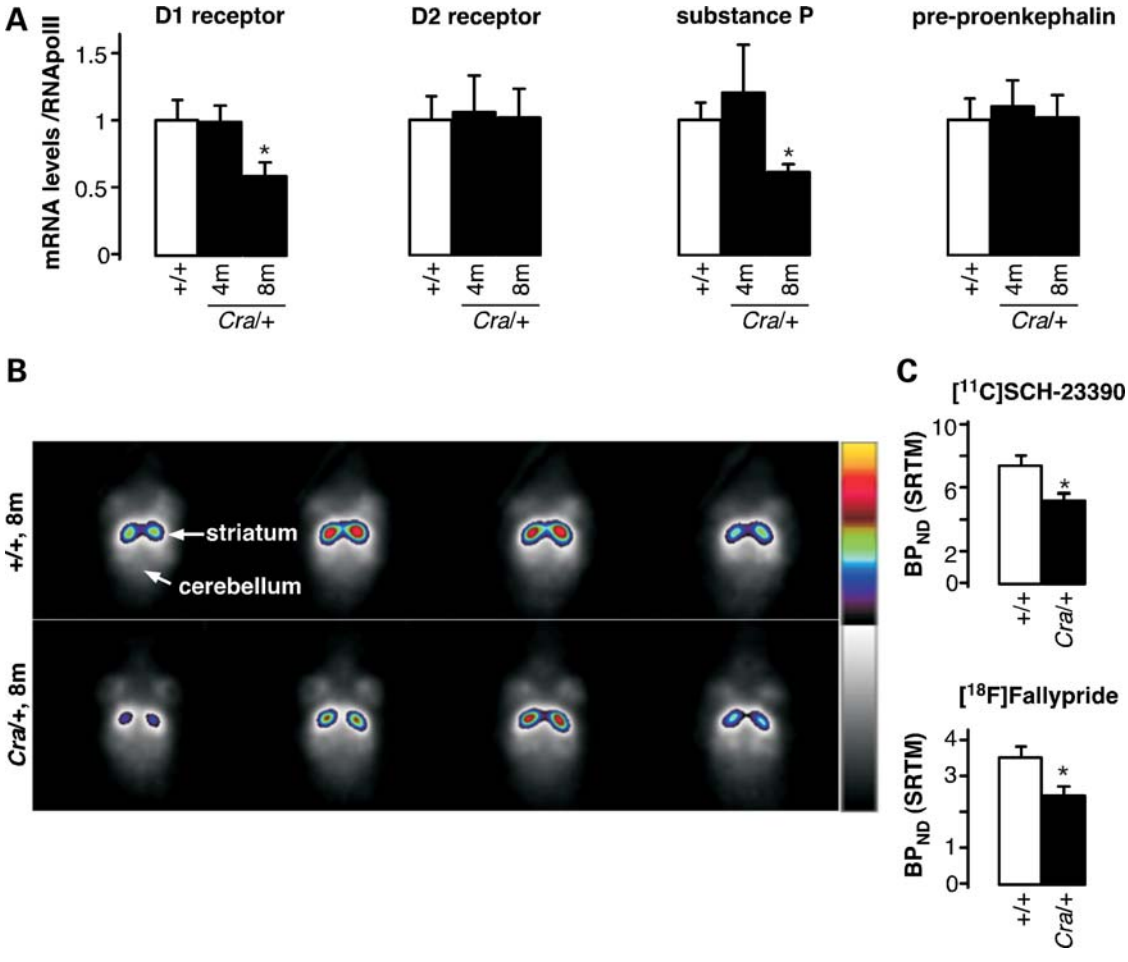

Figure 5. Altered dopamine signalling and binding in the striatum of *Cra*/+ mice. (**A**) mRNA levels of the dopamine D1 and D2 receptor, substance P and pre-proenkephalin in the striatum of wild-type mice (+/+) and heterozygous *Cra*/+ mice at 4 and 8 months of age. $^*P < 0.05$ versus wild-type ($n = 5–7$). (**B**) Representative [^{11}C] SCH-23390 images (all frames averaged together) through the striatum of a wild-type mouse brain (+/+, upper panels) and a heterozygous mouse brain (*Cra*/+, lower panels) are shown. (**C**) Binding potentials (BP_{ND}) of [^{11}C] SCH-23390 ($n = 5$) and [^{18}F] Fallypride ($n = 10$) calculated using SRTM. $^*P < 0.05$ versus wild-type.

arborization, even if bearing a single mutant allele, as revealed using β3-tubulin (neurites) or microtubule associated protein 2 (MAP2) (somatodendritic) immunostaining (Fig. 6F). Quantification revealed a reduction in the complexity of neuritic arborization of dynein mutant striatal neurons that were observed in *Cra*/+ neurons and even more pronounced in *Cra/Cra* neurons (Fig. 6G–H). The length of the longest individual MAP2 positive neurite was dramatically decreased by the presence of the dynein mutation (Fig. 6G). Thus, the dynein mutation led to dramatically impaired neuritic arborization in cultured neurons while sparing survival of these cells, suggesting that this dysfunction caused the overall pathological phenotype.

DISCUSSION

This study provides evidence for the *in vivo* requirement of dynein in the function of the striatum and indicates that this occurs through involvement of cytoplasmic dynein in neuritic arborization. The consequences of these findings are important for neurodegenerative diseases affecting the basal ganglia.

Cra/+ mice suffer from motor and behavioural disturbances through their whole lifespan. we and others have previously shown the occurrence of an early and relatively mild proprioceptive neuropathy in *Cra*/+ mice (26–28), but this limited phenotype does not explain the overall behavioural and locomotor abnormalities observed here. First, muscle weakness is usually observed in patients presenting motor neuropathy, but not in patients affected by a pure sensory neuropathy (40) as in *Cra*/+ mice. Second, behavioural abnormalities, including limb clasping and hyperactivity, rather suggest a central involvement and do not comply with a pure sensory neuropathy. These behavioural abnormalities are suggestive of striatal involvement. Indeed, the early phase of the pathology in mouse models of HD is characterized by an increase in spontaneous motor activity (29–31,41). Similarly, transgenic mice lacking cortical BDNF or conditionally ablated for BDNF at adulthood display hindlimb and forelimb clasping (34,35), and mice deficient in PGC-1α, a transcriptional coactivator involved in the regulation of energy metabolism, also present with limb clasping and hyperactivity (42). Importantly, all these transgenic animals display

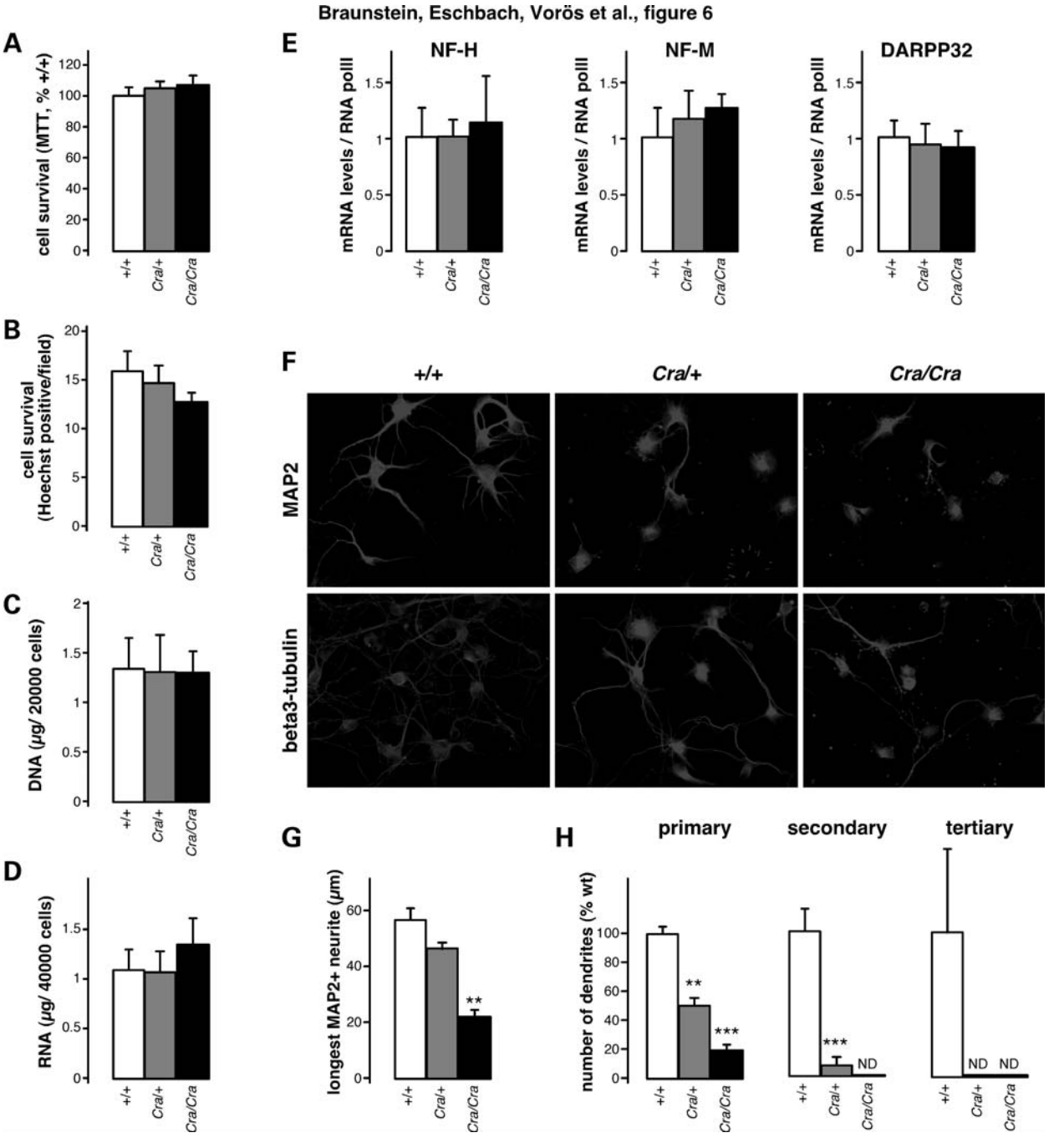

Figure 6. Dramatic defect in dendritic morphology of cultured dynein mutant striatal neurons. (**A** and **B**) Cell survival of primary striata neuronal culture from wild-type embryo (+/+), heterozygous *Cra*/+ embryo and homozygous *Cra/Cra* embryo after 7 days in culture as assessed using MTT reduction assay (A) or direct counting of nuclei (B). (**C** and **D**) DNA (C) and RNA (D) content of primary striata neuronal culture from wild-type embryo (+/+), heterozygous *Cra*/+ embryo and homozygous *Cra/Cra* embryo after 7 days in culture. (**E**) mRNA levels of neurofilament heavy (NF-H) or medium (NF-M) subunits and of DARPP-32 in primary striata neuronal culture from wild-type embryo (+/+), heterozygous *Cra*/+ embryo and homozygous *Cra/Cra* embryo after 7 days in culture. (**F**) Representative microphotographs of MAP2 and β3-tubulin immunostaining of primary striata neuronal culture from wild-type embryo (+/+), heterozygous *Cra*/+ embryo and homozygous *Cra/Cra* embryo. (**G**) Length of longest neurite of individual striatal cells stained by MAP2 antibody from wild-type embryo (+/+), heterozygous *Cra*/+ embryo and homozygous *Cra/Cra* embryo. Total number of cells analysed: +/+108 cells, *Cra*/+162 cells and *Cra/Cra* 81 cells, $^{**}P < 0.01$ versus wild-type (ANOVA followed by Newman–Keuls *post hoc* test). (**H**) Quantification of the number of MAP2 immunopositive primary, secondary and tertiary neurites from wild-type embryo (+/+), heterozygous *Cra*/+ embryo and homozygous *Cra/Cra* embryo. Total number of cells analysed: +/+68 cells, Cra/+126 cells and Cra/Cra 61 cells. $^{**}P < 0.01$ versus wild-type, $^{***}P < 0.001$ versus wild-type (ANOVA followed by Newman–Keuls *post hoc* test).

a clear-cut lesion in the striatum. This is particularly interesting, because the genetic ablation of D1 dopamine receptor expressing cells (that is, within the striatum) yields a motor phenotype very similar to that observed in mutant dynein mice (32). In all, the selective down-regulation of the expression of D1 dopamine receptors, together with striatal atrophy, enlargement of lateral ventricles, decreased binding to either D1 or D2 dopamine receptors and the prominent astrocytosis that we found in the striatum of *Cra*/+ mice suggest that a striatal dysfunction can lead, at least in part, to the stereotyped motor disturbances in these mice.

Gene expression of D1 receptor, as well as binding potential of [^{11}C] SCH-23390, was decreased in *Cra*/+ striatum. In contrast, despite the binding potential of D2 receptor was decreased, its gene expression was unchanged. There are several potential explanations to this discrepancy. First, the binding potential calculated from the PET analysis is a reflection of both the density of available receptor sides and the apparent ligand affinity (43). Since apparent ligand affinity is decreased by competition with the natural ligand, dopamine, an increase in striatal dopamine could, in principle, explain a decreased binding potential observed with PET. This explanation is, however, unlikely in our case because [^{18}F] Fallypride is a high-affinity antagonist radioligand, and therefore less sensitive to changes in synaptic dopamine than agonist radioligands (43). Second, our stereological assessment of substantia nigra suggests that striatal dopaminergic innervation is rather normal in *Cra*/+ striatum. Thus, the lower D2 binding potential observed in *Cra*/+ mice is most likely due to a reduction of D2 receptor binding sites rather than to increased striatal dopamine. Such a decrease might be explained by defects in the various trafficking events that modulate cell surface expression of D2 receptor (44–47). Indeed, given the involvement of dynein in a number of cellular trafficking events, it cannot be excluded that the dynein mutation might directly impair D2 receptor trafficking.

Intriguingly, the behavioural phenotype of *Cra*/+ mice, as well as decreased D1 and D2 ligand binding and striatal atrophy, appeared between 3 and 4 months of age, while astrocytosis and transcriptional repression of D1 receptors were detectable later, after 8 months. The fact that behavioural abnormalities precede marked histopathological and biochemical changes in the striatum is not without precedent. For instance, previous studies reported that motor dysfunction in huntingtin knock-in mice occurred long before any clear signs of striatal lesions (48). We did not detect decreased DARPP-32 neuronal counts showing that the striatal phenotype was not associated with neurodegeneration, but most probably with dendritic atrophy, as suggested by our *in vitro* data. Our results, however, do not exclude the occurrence of a very slow and subtle process of striatal neurodegeneration that would be difficult to detect. Astrocytosis itself might be an astrocyte-autonomous event. Dynein expression and function in astrocytes has been poorly characterized and the elucidation of astrocytic dynein to the phenotype of dynein mutant mice will require the generation of conditional knock-out mice.

Our cell culture experiments show the existence of an intrinsic and massive defect in neuritic morphology of dynein mutant striatal neurons. The defect in neurite outgrowth of dynein mutant neurons is fully consistent with the recently reported critical requirement of dynein itself for dendrite outgrowth in drosophila neurons (49,50) and of the dynein-interacting protein LIS1 in dendrite morphology (51,52). Our data provide further evidence for such an involvement in mammals. The underlying molecular mechanisms remain unclear but might include perturbations of endosomal trafficking as suggested by the requirement for dynein in endosomal trafficking (53,54) and the requirement of endosomal trafficking in dendritic arborization (50,55). Interestingly, such a defect has not been noted by previous investigators that had performed dynein mutant motor neuron cultures (24,56), suggesting that motor neurons of dynein mutant mice were preserved comparatively to striatal neurons. This is in line with very recent transgenic experiments of adult BDNF deprivation that showed a specific sensitivity of MSNs to defects in dendrite morphogenesis when compared with other types of neurons (35). Furthermore, Gertler *et al.* (57) showed that D1 MSNs displayed more primary dendrites than D2 MSNs, suggesting a rationale for the more profound D1 involvement in the striatal pathology of *Cra*/+ mice. In all, our results suggest that the dynein mutation impairs dendritic arborization, and that the pathological consequences are more prominent in the striatum, likely because of a hugely developed dendritic arbour of MSNs.

Previous work in cultured cells had involved dynein and dynactin in different basal ganglia diseases, notably in HD and Perry syndrome. Indeed, huntingtin and its associated protein HAP1 bind to dynein directly, and indirectly, through dynactin subunit P150^{Glued}. Importantly, the disease-causing protein in HD, mutant huntingtin, disrupts these interactions and decreases dynein function (21). Dynactin is also required for huntingtin-dependent transport of BDNF vesicles (22). These results suggested that dynein might be of importance for the survival and/or functioning of striatal neurons. However, most evidence to date of an *in vivo* role for dynein in neurons were based either on overexpression of the dynamitin subunit of dynactin or on overexpression of mutant forms of P150^{Glued}, and mutant huntingtin affects not only retrograde but also anterograde axonal transport (23). Since dynactin and huntingtin have a number of dynein-independent functions, our results provide a direct genetic evidence for a pathophysiological role of dynein in striatal neuron health. Interestingly, cross-breeding dynein mutant mice with an animal model of HD sharply exacerbated the HD-like pathology (58). Most importantly, we observed that dynein mutant mice exhibited other HD-related peripheral phenotypes (59), including increased adiposity and impaired brown adipose thermogenesis (our unpublished data), thus strengthening the analogy between HD animal models and dynein mutant mice.

In summary, our findings provide direct evidence of the involvement of the axonal transport machinery, notably dynein, in the maintenance of striatal function and may have major implications for our understanding of basal ganglia diseases, such as HD and Perry syndrome.

MATERIALS AND METHODS

Animals

Heterozygous *Cra*/+ mice were obtained from Ingenium Pharmaceuticals AG, Martinsried, Germany. They were identified

by tail DNA genotyping as previously described (24). Animals were maintained in a temperature- and humidity-controlled environment on a 12 h light/12 h dark cycle, and received food and water *ad libitum*. For the histological analysis, animals were deeply anaesthetized with 1 mg/kg body weight ketamine chlorhydrate and 0.5 mg/kg body weight xylazine, and transcardially perfused with 4% paraformaldehyde in 0.1 M pH 7.4 phosphate buffer. Tissues were then quickly dissected, post-fixed for 24 h in 4% paraformaldehyde and cryoprotected for 48 h with 30% sucrose in PBS before cryostat sectioning. For the biochemical analysis, animals were sacrificed and tissues were quickly dissected, snap frozen in liquid nitrogen and stored at −80°C until use. Animal manipulation followed current EU regulations and was performed under the supervision of authorized investigators.

Real-time RT–PCR

Total RNA was extracted using Trizol (Invitrogen, Cergy-Pontoise, France) according to the manufacturer's instructions. cDNA synthesis was performed using 1 μg of total RNA (iScript cDNA Synthesis kit; Bio-Rad, Marne La Coquette, France). PCR analysis was carried out as described (27) on a Bio-Rad CFX96 System using iQSYBR Green Supermix. A specific standard curve was performed for each gene in parallel, and each sample was quantified in duplicate. PCR conditions were 3 min at 94°C, followed by 40 cycles of 45 s at 94°C and 10 s at 60°C. Data were analysed using the iCycler software, and normalized to the reference genes encoding either the 18S ribosomal subunit and the RNA polymerase II mRNA. The primer pairs used are provided in Supplementary Material, Table S1.

Testing of motor performance and behaviour

Muscle grip strength was measured using a Bioseb gripmeter (Vitrolles, France) on forelimbs and all limbs. Each assay was performed in triplicate and measurements were averaged. For the behavioural analysis, C3H *Cra*/+ females were crossed with Bl6 males in order to compare with a group of mutant SOD1 (G93A) mice in mixed C3H/Bl6 background analysed in parallel (60). One week before the start of the tests, animals were brought to the behavioural analysis facility; single caged and handled every day. Only male mice were used for the tests. The rotarod test was used to assess motor coordination and balance. Mice had to keep their balance on a rotating rod at a continuous acceleration from 4 to 40 r.p.m. for 300 s (Rotarod Version 1.2.0. MED Associates Inc., St Albans, VT, USA). The time (or latency) it took the mouse to fall off the rod was measured. Each mouse had to perform three trials separated by 15 min each other, and the three trials were averaged. To identify differences in locomotor activity and exploratory behaviour, mice were tested in the open field. In this test, animals were placed at the border of a square arena (50 cm × 50 cm) and allowed to explore the arena freely for 30 min. The arena was divided into three parts, including a border zone (within 8 cm of the wall), a centre zone (inner square of 20 cm × 20 cm) and an intermediate zone. Locomotor activity was assessed by the total distance moved and the average velocity. To determine the exploratory behaviour, the number of rearings within the 30 min was measured. To assess anxiety, mice were evaluated using an elevated plus maze paradigm. The maze was elevated 92 cm above the floor, and consisted of four arms of 30 × 5 cm each, including two opposite 'closed' arms surrounded by dark walls and two opposite 'open' arms exposed without any walls. The centre of the maze was a 5 × 5 cm common area. Each mouse was placed for a single trial at the centre of the maze facing a closed arm, and allowed to explore the maze freely for a period of 5 min. The amount of time (in seconds) spent in both the open arms and closed arms was recorded. To measure reference learning (acquisition) and memory (retention), the Morris water maze was performed. The device consisted of a circular pool of 120 cm diameter, filled with water (25–27°C), which was made opaque by adding 2 l of milk. The pool was divided into four equal-sized quadrants and was surrounded by grey curtains covered with various visual cues, which helped the mice orient their location in the pool. A 10 cm platform was placed in the quadrant A, such that the platform was 1 cm below the water surface and visually indiscernible to the animals. On each trial, mice were allowed to swim for a maximum of 60 s and were released from four different defined positions. If the animal failed to discover the location of the platform in 60 s, it was guided to the platform and then allowed to stay for 30 s. After removal, mice were placed under an infrared lamp and allowed to warm up and dry off. The test was divided into two phases, an acquisition phase (18 trails, 6 per day), followed by a reversal phase during which the platform was moved to the opposite quadrant (12 trails, 6 per day). Escape latency and swum distance were analysed during both acquisition and reversal learning, and two successive trials were averaged into one block. All paths were tracked and analysed with an electronic imaging system (Viewer 2.2.0.55, BIOBSERVE GmbH, Bonn, Germany) at a frequency of 15 Hz and a spatial resolution of 720 × 576 pixels.

Assessment of the striatal and lateral ventricle volume by MRI

MRI was performed in the In-vivo-Imaging Laboratory at the research site of Boehringer Ingelheim Pharma GmbH & Co. KG, Biberach, Germany. MRI data were acquired on a Bruker Biospec 47/40 scanner (Bruker BioSpin, Ettlingen, Germany) at 4.7 T (200 MHz proton resonance frequency). Age- and gender-matched *Cra*/+ and wild-type animals were used ($n = 20$). Acquisitions were performed at 5 and 10 months of age, respectively. Mice were anaesthetized through continuous inhalation of 1.2–1.5% isoflurane (in 70:30 N_2O:O_2) and fixed in a stereotactic head holder. For the anatomical analysis of the mouse brain, contiguous sets of six horizontal T_2-weighted images were acquired using a RARE sequence. Imaging parameters were: TR 2500 ms, TE 12.5 ms, TEeff 50 ms, slice thickness 600 μm (no gap), FOV 28.1 × 25.6 mm, matrix size 256 × 256, RARE factor 8, six averages. Data processing was performed by the in-house developed software package Tissue Classification Software (TCS). For good visualization, the BRUKER data were transformed into a 768 × 768 grid (nearest neighbour interpolation, no filtering). TCS includes mouse-based

drawing tools for tissue/voxel selection. In order to define clearly visible regions, drawing was simplified by a two-level thresholded conventional region-grow algorithm. Following the operator-defined intensity threshold, all connected voxels with respect to their intensity within the predefined range were selected. The analysis was blinded, evaluated by the same experienced investigator. The striatum was identified in four consecutive horizontal slices when compared with the Mouse Brain Library (http://www.mbl.org/mbl_main/atlas.html) between Bregma: −3.24; Interaural: 6.76 and Bregma: −5.04; Interaural: 4.96. The lateral ventricles were identified in the same horizontal sections by semi-automated region growth.

Analysis of brain astrocytosis

Brain sections comprising the anterior part of the caudate nucleus and the putamen were cut on a vibratome at a thickness of 50 μm (Leica Microsystems, Wetzlar, Germany) and were stained by indirect immunofluorescence, using an antibody directed against the specific astrocyte marker GFAP (Santa Cruz Biotechnology, Heidelberg, Germany) following the manufacturer's instructions. Quantitative analysis of immunoreactivity was performed using ImageJ.

Stereological analysis of DARPP-32 and TH-positive neurons

Coronal sections were cut in six series at a thickness of 35 μm throughout the brains using a freezing microtome. One series of free-floating brain sections were processed for immunohistochemistry either with a primary rabbit antibody against DARPP-32 (1:1000, Chemicon, AB 1656) or TH (1:1000, Pelfreez) (61). Stereological estimations of the total number of DARPP-32 positive neurons in the striatum or TH-positive neurons in the substantia nigra pars compacta were performed unilaterally on blind-coded slides with the Computer Assisted Toolbox Software (New CAST) module in VIS software (Visiopharm, Horsholm, Denmark) by applying the optical fractionator principle (62).

Micropet studies

Five wild-type and five *Cra*/+ mice were used for [^{11}C] SCH-23390 PET imaging. Mice were anaesthetized with 1.5% isoflurane vaporized in 1.0 l/min oxygen gas (Vetland, Anesthesia Systems, Louisville, KY, USA). Two mice were placed head to head in the centre of field of view of a dedicated small animal PET scanner (Siemens Preclinical Solutions, Knoxville, TN, USA) yielding a spatial resolution of ∼1.4 mm in the reconstructed images. A 60 min emission scan was performed starting with bolus injection of [^{11}C] SCH-23390 (12 ± 1 MBq) via a tail vein catheter. A heating mat was used to keep the animal warmed over the whole scan time. List-mode data were histogrammed into 64 time frames (30 × 10 s, 10 × 30 s, 10 × 60 s, 10 × 120 s, 4 × 300 s) and reconstructed using OSEM2D. To reveal quantitative images, dead-time correction, decay correction, normalization and attenuation correction were applied to all data sets. Two rectangular regions of interest (ROIs) for the left and the right striata of a size of 1 × 1 mm^2 as well as for the cerebellum (3 × 1.5 mm^2), which was used as reference region, were applied to all data sets. The ROIs were placed on two constitutive transversal slices of the striatum and the cerebellum. Time activity curves for the quantitative analysis were generated using PMOD software 3.0 (PMOD Technologies, Zurich, Switzerland). The simplified reference tissue model (63) was used to calculate the binding potential (BP_{ND}) of [^{11}C] SCH-23390.

For [^{18}F] Fallypride PET measurements, 10 animals of each group (*Cra*/+ and wild-type) were randomly selected at 10 months of age. Animals were anaesthetized through continuous inhalation of 1.2–1.5% isoflurane (in 70:30 N_2O:O_2). PET imaging was performed on a Siemens Inveon PET/CT system (Siemens Preclinical Solutions) using the D2/3 receptor ligand [^{18}F] Fallypride (33,64). After bolus injection of radioactively labelled Fallypride (average activity 11.7 ± 2.0 MBq) through a tail vein catheter, PET data were continuously acquired for 60 min. Afterwards, list mode data were histogrammed into 21 frames (3 × 20 s, 4 × 60 s, 3 × 120 s, 3 × 180 s, 8 × 300 s) and reconstructed using a filtered back-projection algorithm without scatter correction. Quantitative analysis was assessed by SMRT implemented on the Inveon Research Workplace (IRW) software package (Siemens Molecular Imaging, Erlangen, Germany). ROIs were defined on co-registered PET/CT images using IRW.

Striatal neuron culture

Primary striatal neurons were cultured from E15 embryos issued from a cross between two heterozygous *Cra*/+ mice. Neurons from each embryo were cultured separately and genotype was determined *post hoc* by DNA genotyping of remaining embryos tissues. After enzymatic and mechanical dissociation, primary striatal neurons were plated at a density of 2.10^5 cells/ml on 0.1 mg/ml polyornithine precoated culture dishes and grown at 37°C in a humidified atmosphere (5% CO_2/95% air). Culture media were composed of Neurobasal defined medium supplemented with B27, glutamax (2 mM), KCl (25 mM) and gentamycin (50 μg/ml). Primary neurons were cultured for 7 days, and the culture media were changed every 2 days. BDNF treatment (Tocris Bioscience, Ellisville, MO, USA) was performed the seventh day at the indicated concentration for 4 h.

For immunocytochemistry, primary striatal neurons were post-fixed with 4% paraformaldehyde in PBS pH 7.4 and were permeabilized for 30 min in 1% Triton X-100/PBS. Primary antibodies anti-MAP-2 and β3 Tubulin (Millipore, Molsheim, France) were applied overnight, and Rhodamine-conjugated secondary antibody (Jackson Immunoresearch Laboratories, West Grove, PA, USA) was applied for 1 h. Cover slips were mounted in Mowiol solution for observation under a conventional epifluorescence microscope (Nikon, Tokyo, Japan) and pictures were analysed with ImageJ software.

MTT assays

3-(4,5-Dimethylthiazol-2-yl)-2,5-diphenyltetrazolium bromide (MTT) (Sigma-Aldrich, Lyon, France) tests were done with primary striatal neurons cultured in 96-well culture dishes

(Costar, NY, USA). Briefly, MTT was dissolved in PBS (pH 7.2) to obtain a concentration of 5 mg/ml, then diluted 10 times in freshly prepared culture medium and the plates were incubated for 1 h at 37°C. Medium was then removed and dark blue crystals formed during reaction were dissolved by adding 100 µl/well of 0.04 M HCl in isopropyl alcohol. Plates were read on a Bio-Rad 680 micro-ELISA plate-reader, using a wavelength of 490 nm. Results are given in percentage of the +/+ values.

Cell counting

Cultured embryonic striatal neurons' survival was evaluated after nuclei staining with Hoechst 33342 (Sigma-Aldrich). Hoescht solution was dissolved in 100% methanol to obtain a final concentration of 0.5 mg/ml. After paraformaldehyde fixation, cultured embryonic striatal neurons were incubated 30 min with 0.5 µg/ml Hoechst 33342 in 0.1% Triton X-100/PBS and then washed three times in 0.1% Triton X-100/PBS. A total of five embryos of each genotype were analysed and six fields per embryo were randomly photographed on a Nikon fluorescence microscope. The total number of nuclei per field was count. Results represented the average number of nuclei per field.

BDNF ELISA

BDNF ELISA (Promega, Charbonnières-les-Bains, France) was performed as described by the provider.

Statistical analysis

Data are expressed as the mean ± SEM. Statistical analysis was accomplished using non-parametric Student's *t*-test or ANOVA followed by Newman–Keuls multiple comparisons test (PRISM Version 4.0b; GraphPad, San Diego, CA, USA). Differences at $P < 0.05$ were considered significant.

SUPPLEMENTARY MATERIAL

Supplementary Material is available at *HMG* online.

ACKNOWLEDGEMENTS

We acknowledge the skilful technical assistance of Marie-José Ruivo, Annie Picchinenna, Lise Nuss and Caroline Mursch. Pr Ehret helped for behavioural studies. David Kind and Michael Neumaier provided help with MRI and PET imaging. We thank the radiopharmacy group of the University Hospital Tübingen for synthesizing the ^{11}C tracer.

Conflict of Interest statement. None declared.

FUNDING

This work was supported by grants from Fondation pour la Recherche Médicale, Association pour la Recherche sur la Sclérose Latérale Amyotrophique (ARS) and Amyotrophic Lateral Sclerosis Association (grant 1698) to L.D.; and Association Française contre les Myopathies, ARS and Association pour la Recherche et le Développement de Moyens de Lutte contre les Maladies Neurodégénératives to J.-P.L. and by Deutsche Forschungsgemeinschaft (KFO142) to A.C.L. J.L.G.D.A. is the recipient of chaire INSERM/Université de Strasbourg; K.R.-V. held an EFNS Scientific Fellowship at the University of Ulm. Å.P. is supported by grants from the Swedish Research Council.

REFERENCES

1. Morfini, G.A., Burns, M., Binder, L.I., Kanaan, N.M., LaPointe, N., Bosco, D.A., Brown, R.H. Jr, Brown, H., Tiwari, A., Hayward, L. *et al.* (2009) Axonal transport defects in neurodegenerative diseases. *J. Neurosci.*, **29**, 12776–12786.
2. Chevalier-Larsen, E. and Holzbaur, E.L. (2006) Axonal transport and neurodegenerative disease. *Biochim. Biophys. Acta*, **1762**, 1094–1108.
3. Levy, J.R. and Holzbaur, E.L. (2006) Cytoplasmic dynein/dynactin function and dysfunction in motor neurons. *Int. J. Dev. Neurosci.*, **24**, 103–111.
4. LaMonte, B.H., Wallace, K.E., Holloway, B.A., Shelly, S.S., Ascano, J., Tokito, M., Van Winkle, T., Howland, D.S. and Holzbaur, E.L. (2002) Disruption of dynein/dynactin inhibits axonal transport in motor neurons causing late-onset progressive degeneration. *Neuron*, **34**, 715–727.
5. Teuling, E., van Dis, V., Wulf, P.S., Haasdijk, E.D., Akhmanova, A., Hoogenraad, C.C. and Jaarsma, D. (2008) A novel mouse model with impaired dynein/dynactin function develops amyotrophic lateral sclerosis (ALS)-like features in motor neurons and improves lifespan in SOD1-ALS mice. *Hum. Mol. Genet.*, **17**, 2849–2862.
6. Puls, I., Jonnakuty, C., LaMonte, B.H., Holzbaur, E.L., Tokito, M., Mann, E., Floeter, M.K., Bidus, K., Drayna, D., Oh, S.J. *et al.* (2003) Mutant dynactin in motor neuron disease. *Nat. Genet.*, **33**, 455–456.
7. Munch, C., Sedlmeier, R., Meyer, T., Homberg, V., Sperfeld, A.D., Kurt, A., Prudlo, J., Peraus, G., Hanemann, C.O., Stumm, G. *et al.* (2004) Point mutations of the p150 subunit of dynactin (DCTN1) gene in ALS. *Neurology*, **63**, 724–726.
8. Puls, I., Oh, S.J., Sumner, C.J., Wallace, K.E., Floeter, M.K., Mann, E.A., Kennedy, W.R., Wendelschafer-Crabb, G., Vortmeyer, A., Powers, R. *et al.* (2005) Distal spinal and bulbar muscular atrophy caused by dynactin mutation. *Ann. Neurol.*, **57**, 687–694.
9. Wider, C., Dachsel, J.C., Farrer, M.J., Dickson, D.W., Tsuboi, Y. and Wszolek, Z.K. Elucidating the genetics and pathology of Perry syndrome. *J. Neurol. Sci.*, **289**, 149–154.
10. Farrer, M.J., Hulihan, M.M., Kachergus, J.M., Dachsel, J.C., Stoessl, A.J., Grantier, L.L., Calne, S., Calne, D.B., Lechevalier, B., Chapon, F. *et al.* (2009) DCTN1 mutations in Perry syndrome. *Nat. Genet.*, **41**, 163–165.
11. Levy, J.R., Sumner, C.J., Caviston, J.P., Tokito, M.K., Ranganathan, S., Ligon, L.A., Wallace, K.E., LaMonte, B.H., Harmison, G.G., Puls, I. *et al.* (2006) A motor neuron disease-associated mutation in p150Glued perturbs dynactin function and induces protein aggregation. *J. Cell Biol.*, **172**, 733–745.
12. Laird, F.M., Farah, M.H., Ackerley, S., Hoke, A., Maragakis, N., Rothstein, J.D., Griffin, J., Price, D.L., Martin, L.J. and Wong, P.C. (2008) Motor neuron disease occurring in a mutant dynactin mouse model is characterized by defects in vesicular trafficking. *J. Neurosci.*, **28**, 1997–2005.
13. Chevalier-Larsen, E.S., Wallace, K.E., Pennise, C.R. and Holzbaur, E.L. (2008) Lysosomal proliferation and distal degeneration in motor neurons expressing the G59S mutation in the p150Glued subunit of dynactin. *Hum. Mol. Genet.*, **17**, 1946–1955.
14. Lai, C., Lin, X., Chandran, J., Shim, H., Yang, W.J. and Cai, H. (2007) The G59S mutation in p150(glued) causes dysfunction of dynactin in mice. *J. Neurosci.*, **27**, 13982–13990.
15. Berezuk, M.A. and Schroer, T.A. (2007) Dynactin enhances the processivity of kinesin-2. *Traffic*, **8**, 124–129.
16. King, S.J. and Schroer, T.A. (2000) Dynactin increases the processivity of the cytoplasmic dynein motor. *Nat. Cell Biol.*, **2**, 20–24.
17. Lee, S.J., Chae, C. and Wang, M.M. (2009) p150/glued modifies nuclear estrogen receptor function. *Mol. Endocrinol.*, **23**, 620–629.

18. Shrum, C.K., Defrancisco, D. and Meffert, M.K. (2009) Stimulated nuclear translocation of NF-kappaB and shuttling differentially depend on dynein and the dynactin complex. *Proc. Natl Acad. Sci. USA*, **106**, 2647–2652.
19. Li, S.H., Gutekunst, C.A., Hersch, S.M. and Li, X.J. (1998) Interaction of huntingtin-associated protein with dynactin P150Glued. *J. Neurosci.*, **18**, 1261–1269.
20. Li, X.J., Li, S.H., Sharp, A.H., Nucifora, F.C. Jr, Schilling, G., Lanahan, A., Worley, P., Snyder, S.H. and Ross, C.A. (1995) A huntingtin-associated protein enriched in brain with implications for pathology. *Nature*, **378**, 398–402.
21. Caviston, J.P., Ross, J.L., Antony, S.M., Tokito, M. and Holzbaur, E.L. (2007) Huntingtin facilitates dynein/dynactin-mediated vesicle transport. *Proc. Natl Acad. Sci. USA*, **104**, 10045–10050.
22. Gauthier, L.R., Charrin, B.C., Borrell-Pages, M., Dompierre, J.P., Rangone, H., Cordelieres, F.P., De Mey, J., MacDonald, M.E., Lessmann, V., Humbert, S. *et al.* (2004) Huntingtin controls neurotrophic support and survival of neurons by enhancing BDNF vesicular transport along microtubules. *Cell*, **118**, 127–138.
23. Morfini, G.A., You, Y.M., Pollema, S.L., Kaminska, A., Liu, K., Yoshioka, K., Bjorkblom, B., Coffey, E.T., Bagnato, C., Han, D. *et al.* (2009) Pathogenic huntingtin inhibits fast axonal transport by activating JNK3 and phosphorylating kinesin. *Nat. Neurosci.*, **12**, 864–871.
24. Hafezparast, M., Klocke, R., Ruhrberg, C., Marquardt, A., Ahmad-Annuar, A., Bowen, S., Lalli, G., Witherden, A.S., Hummerich, H., Nicholson, S. *et al.* (2003) Mutations in dynein link motor neuron degeneration to defects in retrograde transport. *Science*, **300**, 808–812.
25. Perlson, E., Jeong, G.B., Ross, J.L., Dixit, R., Wallace, K.E., Kalb, R.G. and Holzbaur, E.L. (2009) A switch in retrograde signaling from survival to stress in rapid-onset neurodegeneration. *J. Neurosci.*, **29**, 9903–9917.
26. Ilieva, H.S., Yamanaka, K., Malkmus, S., Kakinohana, O., Yaksh, T., Marsala, M. and Cleveland, D.W. (2008) Mutant dynein (Loa) triggers proprioceptive axon loss that extends survival only in the SOD1 ALS model with highest motor neuron death. *Proc. Natl Acad. Sci. USA*, **105**, 12599–12604.
27. Dupuis, L., Fergani, A., Braunstein, K.E., Eschbach, J., Holl, N., Rene, F., Gonzalez De Aguilar, J.L., Zoerner, B., Schwalenstocker, B., Ludolph, A.C. *et al.* (2009) Mice with a mutation in the dynein heavy chain 1 gene display sensory neuropathy but lack motor neuron disease. *Exp. Neurol.*, **215**, 146–152.
28. Chen, X.J., Levedakou, E.N., Millen, K.J., Wollmann, R.L., Soliven, B. and Popko, B. (2007) Proprioceptive sensory neuropathy in mice with a mutation in the cytoplasmic Dynein heavy chain 1 gene. *J. Neurosci.*, **27**, 14515–14524.
29. Luesse, H.G., Schiefer, J., Spruenken, A., Puls, C., Block, F. and Kosinski, C.M. (2001) Evaluation of R6/2 HD transgenic mice for therapeutic studies in Huntington's disease: behavioral testing and impact of diabetes mellitus. *Behav. Brain Res.*, **126**, 185–195.
30. Schiefer, J., Landwehrmeyer, G.B., Luesse, H.G., Sprunken, A., Puls, C., Milkereit, A., Milkereit, E. and Kosinski, C.M. (2002) Riluzole prolongs survival time and alters nuclear inclusion formation in a transgenic mouse model of Huntington's disease. *Mov. Disord.*, **17**, 748–757.
31. Bolivar, V.J., Manley, K. and Messer, A. (2004) Early exploratory behavior abnormalities in R6/1 Huntington's disease transgenic mice. *Brain Res.*, **1005**, 29–35.
32. Gantois, I., Fang, K., Jiang, L., Babovic, D., Lawrence, A.J., Ferreri, V., Teper, Y., Jupp, B., Ziebell, J., Morganti-Kossmann, C.M. *et al.* (2007) Ablation of D1 dopamine receptor-expressing cells generates mice with seizures, dystonia, hyperactivity, and impaired oral behavior. *Proc. Natl Acad. Sci. USA*, **104**, 4182–4187.
33. Siessmeier, T., Zhou, Y., Buchholz, H.G., Landvogt, C., Vernaleken, I., Piel, M., Schirrmacher, R., Rosch, F., Schreckenberger, M., Wong, D.F. *et al.* (2005) Parametric mapping of binding in human brain of D2 receptor ligands of different affinities. *J. Nucl. Med.*, **46**, 964–972.
34. Baquet, Z.C., Gorski, J.A. and Jones, K.R. (2004) Early striatal dendrite deficits followed by neuron loss with advanced age in the absence of anterograde cortical brain-derived neurotrophic factor. *J. Neurosci.*, **24**, 4250–4258.
35. Rauskolb, S., Zagrebelsky, M., Dreznjak, A., Deogracias, R., Matsumoto, T., Wiese, S., Erne, B., Sendtner, M., Schaeren-Wiemers, N., Korte, M. *et al.* (2010) Global deprivation of brain-derived neurotrophic factor in the CNS reveals an area-specific requirement for dendritic growth. *J. Neurosci.*, **30**, 1739–1749.
36. Santi, S., Cappello, S., Riccio, M., Bergami, M., Aicardi, G., Schenk, U., Matteoli, M. and Canossa, M. (2006) Hippocampal neurons recycle BDNF for activity-dependent secretion and LTP maintenance. *EMBO J.*, **25**, 4372–4380.
37. Zhou, P., Porcionatto, M., Pilapil, M., Chen, Y., Choi, Y., Tolias, K.F., Bikoff, J.B., Hong, E.J., Greenberg, M.E. and Segal, R.A. (2007) Polarized signaling endosomes coordinate BDNF-induced chemotaxis of cerebellar precursors. *Neuron*, **55**, 53–68.
38. Bogush, A., Pedrini, S., Pelta-Heller, J., Chan, T., Yang, Q., Mao, Z., Sluzas, E., Gieringer, T. and Ehrlich, M.E. (2007) AKT and CDK5/p35 mediate brain-derived neurotrophic factor induction of DARPP-32 in medium size spiny neurons in vitro. *J. Biol. Chem.*, **282**, 7352–7359.
39. Gokce, O., Runne, H., Kuhn, A. and Luthi-Carter, R. (2009) Short-term striatal gene expression responses to brain-derived neurotrophic factor are dependent on MEK and ERK activation. *PLoS ONE*, **4**, e5292.
40. Auer-Grumbach, M. (2008) Hereditary sensory neuropathy type I. *Orphanet J. Rare Dis.*, **3**, 7.
41. Reddy, P.H., Williams, M., Charles, V., Garrett, L., Pike-Buchanan, L., Whetsell, W.O. Jr, Miller, G. and Tagle, D.A. (1998) Behavioural abnormalities and selective neuronal loss in HD transgenic mice expressing mutated full-length HD cDNA. *Nat. Genet.*, **20**, 198–202.
42. Lin, J., Wu, P.H., Tarr, P.T., Lindenberg, K.S., St-Pierre, J., Zhang, C.Y., Mootha, V.K., Jager, S., Vianna, C.R., Reznick, R.M. *et al.* (2004) Defects in adaptive energy metabolism with CNS-linked hyperactivity in PGC-1alpha null mice. *Cell*, **119**, 121–135.
43. Laruelle, M. (2000) Imaging synaptic neurotransmission with in vivo binding competition techniques: a critical review. *J. Cereb. Blood Flow Metab.*, **20**, 423–451.
44. Xiao, M.F., Xu, J.C., Tereshchenko, Y., Novak, D., Schachner, M. and Kleene, R. (2009) Neural cell adhesion molecule modulates dopaminergic signaling and behavior by regulating dopamine D2 receptor internalization. *J. Neurosci.*, **29**, 14752–14763.
45. Namkung, Y., Dipace, C., Urizar, E., Javitch, J.A. and Sibley, D.R. (2009) G protein-coupled receptor kinase-2 constitutively regulates D2 dopamine receptor expression and signaling independently of receptor phosphorylation. *J. Biol. Chem.*, **284**, 34103–34115.
46. Tirotta, E., Fontaine, V., Picetti, R., Lombardi, M., Samad, T.A., Oulad-Abdelghani, M., Edwards, R. and Borrelli, E. (2008) Signaling by dopamine regulates D2 receptors trafficking at the membrane. *Cell Cycle*, **7**, 2241–2248.
47. Kim, O.J., Ariano, M.A., Namkung, Y., Marinec, P., Kim, E., Han, J. and Sibley, D.R. (2008) D2 dopamine receptor expression and trafficking is regulated through direct interactions with ZIP. *J. Neurochem.*, **106**, 83–95.
48. Menalled, L.B., Sison, J.D., Wu, Y., Olivieri, M., Li, X.J., Li, H., Zeitlin, S. and Chesselet, M.F. (2002) Early motor dysfunction and striosomal distribution of huntingtin microaggregates in Huntington's disease knock-in mice. *J. Neurosci.*, **22**, 8266–8276.
49. Zheng, Y., Wildonger, J., Ye, B., Zhang, Y., Kita, A., Younger, S.H., Zimmerman, S., Jan, L.Y. and Jan, Y.N. (2008) Dynein is required for polarized dendritic transport and uniform microtubule orientation in axons. *Nat. Cell Biol.*, **10**, 1172–1180.
50. Satoh, D., Sato, D., Tsuyama, T., Saito, M., Ohkura, H., Rolls, M.M., Ishikawa, F. and Uemura, T. (2008) Spatial control of branching within dendritic arbors by dynein-dependent transport of Rab5-endosomes. *Nat. Cell Biol.*, **10**, 1164–1171.
51. Fleck, M.W., Hirotsune, S., Gambello, M.J., Phillips-Tansey, E., Suares, G., Mervis, R.F., Wynshaw-Boris, A. and McBain, C.J. (2000) Hippocampal abnormalities and enhanced excitability in a murine model of human lissencephaly. *J. Neurosci.*, **20**, 2439–2450.
52. Liu, Z., Steward, R. and Luo, L. (2000) Drosophila Lis1 is required for neuroblast proliferation, dendritic elaboration and axonal transport. *Nat. Cell Biol.*, **2**, 776–783.
53. Murray, J.W. and Wolkoff, A.W. (2003) Roles of the cytoskeleton and motor proteins in endocytic sorting. *Adv. Drug Deliv. Rev.*, **55**, 1385–1403.
54. Aniento, F., Emans, N., Griffiths, G. and Gruenberg, J. (1993) Cytoplasmic dynein-dependent vesicular transport from early to late endosomes. *J. Cell Biol.*, **123**, 1373–1387.
55. Jan, Y.N. and Jan, L.Y. (2010) Branching out: mechanisms of dendritic arborization. *Nat. Rev. Neurosci.*, **11**, 316–328.
56. Kieran, D., Hafezparast, M., Bohnert, S., Dick, J.R., Martin, J., Schiavo, G., Fisher, E.M. and Greensmith, L. (2005) A mutation in dynein rescues

axonal transport defects and extends the life span of ALS mice. *J. Cell Biol.*, **169**, 561–567.
57. Gertler, T.S., Chan, C.S. and Surmeier, D.J. (2008) Dichotomous anatomical properties of adult striatal medium spiny neurons. *J. Neurosci.*, **28**, 10814–10824.
58. Ravikumar, B., Acevedo-Arozena, A., Imarisio, S., Berger, Z., Vacher, C., O'Kane, C.J., Brown, S.D. and Rubinsztein, D.C. (2005) Dynein mutations impair autophagic clearance of aggregate-prone proteins. *Nat. Genet.*, **37**, 771–776.
59. Weydt, P., Pineda, V.V., Torrence, A.E., Libby, R.T., Satterfield, T.F., Lazarowski, E.R., Gilbert, M.L., Morton, G.J., Bammler, T.K., Strand, A.D. *et al.* (2006) Thermoregulatory and metabolic defects in Huntington's disease transgenic mice implicate PGC-1alpha in Huntington's disease neurodegeneration. *Cell Metab.*, **4**, 349–362.
60. Teuchert, M., Fischer, D., Schwalenstoecker, B., Habisch, H.J., Bockers, T.M. and Ludolph, A.C. (2006) A dynein mutation attenuates motor neuron degeneration in SOD1(G93A) mice. *Exp. Neurol.*, **198**, 271–274.
61. Bode, F.J., Stephan, M., Suhling, H., Pabst, R., Straub, R.H., Raber, K.A., Bonin, M., Nguyen, H.P., Riess, O., Bauer, A. *et al.* (2008) Sex differences in a transgenic rat model of Huntington's disease: decreased 17beta-estradiol levels correlate with reduced numbers of DARPP32+ neurons in males. *Hum. Mol. Genet.*, **17**, 2595–2609.
62. West, M.J., Slomianka, L. and Gundersen, H.J. (1991) Unbiased stereological estimation of the total number of neurons in the subdivisions of the rat hippocampus using the optical fractionator. *Anat. Rec.*, **231**, 482–497.
63. Lammertsma, A.A. and Hume, S.P. (1996) Simplified reference tissue model for PET receptor studies. *Neuroimage*, **4**, 153–158.
64. Yakushev, I., Hammers, A., Fellgiebel, A., Schmidtmann, I., Scheurich, A., Buchholz, H.G., Peters, J., Bartenstein, P., Lieb, K. and Schreckenberger, M. (2009) SPM-based count normalization provides excellent discrimination of mild Alzheimer's disease and amnestic mild cognitive impairment from healthy aging. *Neuroimage*, **44**, 43–50.